RSC Advances

# Effect of Mn doping on electrochemical active of hybrid CuO/Cu(OH)2 electrodes



| | |
|---|---|
| Journal: | *RSC Advances* |
| Manuscript ID: | RA-ART-01-2015-001093.R2 |
| Article Type: | Paper |
| Date Submitted by the Author: | 18-Mar-2015 |





| | |
|---|---|
| Complete List of Authors: | Shinde, Surendra; Shivaji University, Kolhapur, Department of Physics<br>Dubal, deepak; Gwangju Institute of Science and Technology, School of Materials Science and Engineering<br>Ghodake, G S; Kyungpook National University,, Department of Environment Engineering,<br>Kim, Sungyeol; Dongguk University-Seoul, Jung-gu,100-715, Seoul, Korea, Department of Biological and Environmental Science<br>Gomez-Romero, Pedro; Catalan Institute of Nanoscience and Nanotechnology, ICN2 (CSIC-CERCA), Campus UAB, E-08193 Bellaterra, Barcelona, Spain, Catalan Institute of Nanoscience and Nanotechnology, ICN2 (CSIC-CERCA), Campus UAB, E-08193 Bellaterra, Barcelona, Spain<br>Fulari, V; Shivaji University, Kolhapur, Physics |

# Influence of Mn incorporation on supercapacitive properties of hybrid CuO/$Cu(OH)_2$ electrodes

*Surendra K. Shinde*[a], *Deepak P. Dubal*[b], *Gajanan S. Ghodake*[c], *Pedro Gomez-Romero*[b], *Sungyeol Kim*[c], *Vijay J. Fulari*[a*]

[a]Holography and Materials Research Laboratory, Department of Physics, Shivaji University, Kolhapur-416 004, Maharashtra, India

[b]Catalan Institute of Nanoscience and Nanotechnology, ICN2 (CSIC-CERCA), Campus UAB, E-08193 Bellaterra, Barcelona, Spain

[c]Department of Biological and Environmental Science,Dongguk University-Seoul, Jung-gu,100-715, Seoul, Korea

***Corresponding Author**

Prof. Vijay J. Fulari

E-mail address: vijayfulari@gmail.com

Tel.: +91 231 2609224, Fax: +91 231 2690533

**Abstract**

Here, we are presenting the effect of Mn doping on supercapacitive properties of $CuO/Cu(OH)_2$ hybrid electrodes. Briefly, Mn doped $CuO/Cu(OH)_2$ ($Mn:CuO/Cu(OH)_2$) thin films have been synthesized by successive ionic layer adsorption and reaction (SILAR) method which are further characterized by different physiochemical techniques. Our results revealed the formation of hybrid $CuO/Cu(OH)_2$ thin films with significant morphological deviation through Mn doping. Moreover, considerable positive effect of Mn doping on electrochemical properties of hybrid $CuO/Cu(OH)_2$ electrodes have been witnessed. Later, the results suggest that at 3% Mn doping in $CuO/Cu(OH)_2$ electrodes with nanoflower-like nanostructure exhibits highest specific capacitance. The maximum specific capacitance achieved for 3% $Mn:CuO/Cu(OH)_2$ hybrid electrode is 600 $Fg^{-1}$ at 5 $mVs^{-1}$ in 1M $Na_2SO_4$ electrolyte. Additionally, Ragone plot confirms the potential of $Mn:CuO/Cu(OH)_2$ hybrid electrode for electrical energy storage applications.

## 1. Introduction:

Transition metal oxides are the basis of a variety of functional materials with great scientific and industrial significance, such as in lithium-ion batteries [1, 2], solar cells [3], biomedicine [4], sensing [5], or catalysis [6]. These materials show an ever increasing range of structural motifs, and are the key components of a growing number of hybrids and composites. Transition metal oxides with reversible electrochemical properties are probable candidates for energy storage applications in particular for supercapacitors [3-8]. Among different transition metal oxides, cupric oxide (CuO) and cuprous oxide ($Cu_2O$) are indisputably an attractive choice, since they are copious, environmentally benign and cheap in comparison with other investigated systems [9-11]. However, pure CuO and $Cu(OH)_2$ electrodes suffer from poor cyclability and low capacity, which are mainly caused by their low conductivity and by the large volume change during charge/discharge cycles [12-14]. Currently, the preparation of ordered self-assembly of nanoscale building blocks into different architectures has become a hot topic in the field of energy storage materials. Such nanoscale building blocks enhance the surface area and well-ordered pores support the adsorption and transportation of chemical agents, which result in better electrochemical performance of the electrodes. Fabrication of nanostructured electrodes mainly depends on the synthetic method. In present investigation, we have focused on the ability to control the shape of nanocrystals by using a low-cost chemical method. Copper oxides (CuO) have been synthesized using various methods such as electrodeposition [15], hydrothermal [16], precipitation method [17, 18], and chemical bath deposition [19, 20], as well as SILAR method [21]. Among different chemical methods, successive ionic layer adsorption and reaction (SILAR) is a very simple, inexpensive and attractive method.

In order to improve the pseudocapacitive properties of plain copper oxide, the addition of other transition metal oxides has been attempted. Several efforts can be found in the literature on the incorporation of Li in CuO [22] for optical applications, Mn in CuO [23] for magnetic application, Ru in CuO [24] for supercapacitor application, Mn in $Cu_2O$ [25] for semiconducting oxide and K in CuO [26], for lithium ion batteries. Still, there is huge room for investigation of incorporation of different metals in CuO and testing for different applications. However, to the best of our knowledge there is no report on the influence of incorporation of Mn on the supercapacitive properties of hybrid $CuO/Cu(OH)_2$ electrodes.

In the present work, we have studied and report the effect of Mn doping on physiochemical properties and subsequent effect on supercapacitive performance of $CuO/Cu(OH)_2$ hybrid electrodes. In details, $CuO/Cu(OH)_2$ hybrid thin films with different Mn doping concentration have been synthesized by successive ionic layer adsorption an reaction (SILAR) method. Further, the effect of different Mn doping concentrations on physiochemical properties of $CuO/Cu(OH)_2$ hybrid films have been systematically investigated by different characterization techniques. Later, the supercapacitive properties of Mn doped $CuO/Cu(OH)_2$ hybrid electrodes are investigated by cyclic voltammetry, galvanostatic charge/discharge and electrochemical impedance techniques.

## 2. Experimental

### 2.1 Synthesis of CuO thin films

For the deposition of Mn doped $CuO/Cu(OH)_2$ thin films, 0.1 M copper sulfate ($CuSO_4$) and 0.1 M Manganese sulfate ($MnSO_4$) were used as sources of copper and manganese species whereas 0.1 M sodium hydroxide (NaOH) was used as anionic precursor. In order to dope Mn in $CuO/Cu(OH)_2$ hybrid thin films, three different concentrations (1, 3 and 5 at %) of manganese

sulfate were selected. Well cleaned stainless steel substrate was immersed in a cationic precursor solution ($CuSO_4$+$MnSO_4$) for 20s for the adsorption of $Cu^{2+}$ and $Mn^{2+}$ species on the substrate surface. The substrate was rinsed in double distilled water for 5s to remove loosely bound species of $Cu^{2+}$ and $Mn^{2+}$ species. Then, the substrate was immersed in anionic precursor solution (NaOH) which was kept at 300 K for 20s to form a layer of copper oxide material. Rinsing the substrate again in double distilled water for 10s separates out the excess or unreached species. Thus one SILAR cycle of Mn doped CuO/$Cu(OH)_2$ doped hybrid film was completed. Several such SILAR cycles were repeated in order to get the final desired thickness of Mn:(CuO/$Cu(OH)_2$) thin films.

**2.2 Characterization techniques**

Structural studies of Mn doped and undoped CuO/$Cu(OH)_2$ films was carried out with X-ray diffractometer (XRD) using Cu-$K_\alpha$ radiation (K=1.54Å). The film surface morphology was characterized by scanning electron microscopy (FEI Quanta 650F Environmental SEM) with attached Energy-dispersive X-ray spectroscopy (EDAX). The electrochemical performance was analyzed using CHI-660-D electrochemical workstation. The electrochemical measurements were carried out using three electrode cell configurations with Mn doped or undoped CuO/$Cu(OH)_2$ as the working electrode, platinum as the counter electrode and Ag/AgCl as the reference electrode with 1 M $Na_2SO_4$ as the electrolyte. Electrochemical impedance measurements were carried out between 1 Hz and 100 MHz with AC amplitude of 5 mV and bias potential of 0.33V.

**3. Results and discussions**

**3.1Structural analysis**

Fig.1 shows the XRD patterns of the Mn doped and undoped CuO/$Cu(OH)_2$ hybrid thin films on steel substrate. From XRD patterns the formation of hybrid CuO/($Cu(OH)_2$ thin films is confirmed in both Mn doped and undoped samples without any other impurity. The peaks corresponding to (021), (112), (110), (002), (002 -111), (111 200), (-202) and (150 132) planes for all samples can be perfectly indexed to monoclinic-phase CuO (JCPDS card No. 80-0076) and orthorhombic phase of $Cu(OH)_2$ (JCPDS card No. 72-0140). It is also interesting to note that, all the XRD patterns for Mn doped and undoped samples are identical suggesting that incorporation Mn does not change the main crystal structure of CuO/$Cu(OH)_2$ hybrid material. Thus, the XRD patterns reveal the formation of pure (CuO/$Cu(OH)_2$) hybrid with polycrystalline monoclinic structure. The average crystallite size is calculated from the line broadening using Scherrer formula: (1)

$$D = \frac{K\lambda}{\beta \cos\theta} \qquad (1)$$

where K is the shape factor, $\lambda$ is wavelength of $CuK_\alpha$ radiation, β is the full width at half maximum (FWHM) and it represents the instruments broadening and θ is the angle of Bragg diffraction. The average crystallite size of Mn doped undoped CuO/$Cu(OH)_2$ is found to be increased from 7 nm to 14 nm with doping percentage. The average crystallite size slightly increases with increasing Mn doping percentage which may be due to the high ionic mobility, low activation energy and small radius of the Mn ions. Due to the low activation energy it is easier for these ions to transfer from trap sites to nucleation sites during the crystal growth process leading to larger crystallite size [22-24]. Raman spectrum of CuO/$Cu(OH)_2$ was also performed which further confirms the formation of the hybrid material (Supporting information S1).

### 3.2 FTIR analysis

The FTIR spectra of Mn doped and undopedCuO/$Cu(OH)_2$ hybrid thin films have been presented in Fig. 2. As seen from figure, four characteristic strong peaks at 505 $cm^{-1}$, 592 $cm^{-1}$ associated with the Cu-O vibrations of monoclinic CuO and 1121 $cm^{-1}$, 1360 $cm^{-1}$ related to Cu-OH vibration of orthorhombic phase of $Cu(OH)_2$. The peaks centered at 505 $cm^{-1}$, demonstrate red shift and the peak at 592 $cm^{-1}$ shows blue shift compared with the reported values (429, 502, and 591 $cm^{-1}$) [27] with the doping of Mn. The observed red and blue shifts due to Mn-doping may be related to the surface defects. The broad peak at about 3404 $cm^{-1}$ is related to the O-H stretching of hydroxyl group present on the surface of the thin films, which is further confirmed by the band at about 1628 $cm^{-1}$. Notably, in 3% Mn doped CuO($Cu(OH)_2$ sample, the peak associated to Cu-OH group is sharper as compared with other samples suggesting presence of more defects. Thus, FTIR analyses further confirms the formation of hybrid CuO/$Cu(OH)_2$ material with Mn doped and undoped samples which support the XRD results.

### 3.3 Surface morphology analysis

Surface morphologies of Mn doped and undoped CuO/$Cu(OH)_2$ hybrid thin films are presented in Fig. 3. From SEM micrographs, it is observed that the entire substrate surface is covered with different nanostructures such as nanopetals, nanoflakes and nanoflowers for both doped and undoped CuO/$Cu(OH)_2$ films. Remarkably, the nanostructure of pure CuO/$Cu(OH)_2$ thin film was significantly changed from nanopetals to nanoflowers with different doping percentage. Fig. 3 (a, b) shows the formation of well-arranged hierarchical nanopetals which look uniformly spread all over the substrate. These clusters of small nanopetals generate abundant space, which ensures an easier electrolyte ion transport and more superficial electro-active species. With the incorporation of 1 wt% of Mn in CuO/$Cu(OH)_2$, the morphology is

considerably changed from nanopetals to very thin nanosheets interconnected to each other forming nanoflakes-like network (see Fig.3 (c, d)), which would be beneficial for exchange of ions in the electrolyte. Further increase in Mn doping to 3 wt% causes the formation of $CuO/Cu(OH)_2$ nanoflowers composed of large number of very small and tiny flakes as seen from Fig. 3 (e, f), which can provide a high volumetric specific surface area and good mass transport property, generate pores and crevices which allow large surface area for easy diffusion of the electrolyte when used in supercapacitors. Much difference in the surface morphology of $CuO/Cu(OH)_2$ was not observed for further increase in Mn doping concentration to 5 wt% (Fig. 3 (g, h)). Thus, it is summarized that, Mn incorporation in $CuO/Cu(OH)_2$ considerably affects the surface properties of thin films. Insert of Fig. 3 shows EDAX spectra for undoped and doped $CuO/Cu(OH)_2$ thin films. The strong peaks of Cu, O and Mn were found in spectra confirming the existence of Mn in $CuO/Cu(OH)_2$ hybrid films.

We have made an attempt to clarify the formation of the nanopetals, nanoflakes to nanoflowers-like morphology in a graphic approach. Fig. 4 shows the plausible mechanism for the development of undoped and Mn doped $CuO/Cu(OH)_2$ hybrid electrode with special nanostructures. The formation mechanism of the pure and Mn doped $CuO/Cu(OH)_2$ different nanostructures includes the following steps: nucleation, coalescence, growth and final oriented attachment. Mechanism is quite clear; to begin with, as the substrate dipped in copper sulfate and/or manganese sulfate precursors, $Cu^{2+}$ and/or $Mn^{2+}$ ions adsorbed on the substrate due to the electrostatic or chemical forces of attraction. Further, immersion of substrate with pre-adsorbed $Cu^{2+}$and/or $Mn^{2+}$ ions in NaOH solution causes the formation of $CuO/Cu(OH)_2$ which can acts as nucleation center on the substrate surface. Perhaps, the primary nucleation centers were locked on substrates, not allowing the intensification at other routes and only allowing extension

of initially grown materials thus the formation of large crystal at primary phase and then nanostructures such as nanopetals, nanoflakes, nanoflowers etc. with a multiplicity of orientations [28-31].

### 3.4 Electrochemical supercapacitive properties

Fig. 5 (a-c) shows the cyclic voltammetry (CV) curves of Mn doped $CuO/Cu(OH)_2$ hybrid electrodes at the scan rates of 5-100 $mVs^{-1}$. It is seen that, as Mn doping percentage in $CuO/Cu(OH)_2$ increases the current under curve increases till 3 % Mn doping concentration (for reference CV of $CuO/Cu(OH)_2$, see supporting information S2). Later, there is a decrease in the current under the curve. These observations are attributed to the morphological variation of $CuO/Cu(OH)_2$ thin films due to Mn doping. Initial nanopetal-like morphology of $CuO/Cu(OH)_2$ changes to nanoflakes at 1 % Mn doping which further changes to nanoflower at 3 % Mn doping. Such nanoflower-like nanostructure composed of thin nanoflakes can provide more electro-active sites compared to other nanostructures which consequently increases the current under the curve. The specific capacitance of undoped and Mn doped $CuO/Cu(OH)_2$ hybrid electrodes can be calculated by the following equation:

$$C = \frac{1}{mv(V_c - V_a)} \int_{V_a}^{V_c} I(V)dv \qquad (2)$$

where'C' is the specific capacitance ($Fg^{-1}$), '*v*' is the potential scan rate ($mVs^{-1}$), $V_c$-$V_a$ is the potential range (0 to +0.6 V/SCE), 'I' denote the response current (mA) and m is the deposited weight of material on the electrode dipped in the electrolyte. The maximum values of specific capacitances are found to be 192 $Fg^{-1}$ (for undoped), 210 $Fg^{-1}$ (1 % Mn), 600 $Fg^{-1}$ (3 % Mn) and 280 $Fg^{-1}$ (5 % Mn) doped $CuO/Cu(OH)_2$ at 5 $mVs^{-1}$ scan rate, respectively. The highest specific

capacitance for 3 % Mn doped CuO/$Cu(OH)_2$ electrode may be attributed to surface morphology and increased conductivity of CuO/$Cu(OH)_2$ thin films. Several reports are available on supercapacitive properties of CuO thin films. For instance, Dubal et al. [32] reported a specific capacitance of 396 $Fg^{-1}$ for CuO thin film deposited by chemical bath deposition method. Hsu et al. [33] prepared lotus-like CuO/$Cu(OH)_2$ hybrid electrode by cost-effective liquid-solid reaction and reported a maximum specific capacitance of 278 $Fg^{-1}$. The enhancement of the specific capacitance of the flowerlike CuO/$Cu(OH)_2$ hybrid is mainly attributed to the effective utilization of CuO/$Cu(OH)_2$ due to the thin superstructures. Fig. 5 (d) shows the variation of specific capacitance of undoped and Mn doped CuO/$Cu(OH)_2$ with scan rate. The results show that, the specific capacitance decreases with increase in scan rate. The decrease in capacitance is attributed to the presence of inner active sites that are unable to sustain the redox transitions completely at higher scan rates [34].

Galvanostatic charge-discharge at different current densities were evaluated to understand the rate capability of the obtained undoped and Mn doped CuO/$Cu(OH)_2$electrodes and are presented in Fig. 6 (a-c). The shapes of charging and discharging curves were not ideal straight lines, confirming the expected involvement of a pseducapacitive contribution. It is very interesting to note that, the discharge curves for all Mn doped CuO samples show very low '*iR*' drop suggesting high conductivity of the electrode material which might be due to incorporation of Mn in CuO/$Cu(OH)_2$ as well as their unique nanostructures (for reference charge/discharge curves of CuO/$Cu(OH)_2$, see supporting information S3). Moreover, the charging segments were nearly symmetric to their corresponding discharging counter parts, which indicate the high reversibility of Mn:CuO/$Cu(OH)_2$ hybrid electrodes. Further, the specific energy and specific power were extracted from the charge/discharge curves. Fig. 6 (d) shows a Ragone plot

displaying the good values of specific energy and specific power for undoped and Mn doped $CuO/Cu(OH)_2$ electrodes. The specific energy for undoped and Mn doped $CuO/Cu(OH)_2$ electrodes is in the range between 10-50 Wh/kg while specific power is between 0.700-3.1 kW/kg. The values of specific energy and specific power are quite impressive which eventually confirms the potential of $Mn:CuO/Cu(OH)_2$ hybrid electrode for high performance energy storage devices. Fig. 7 shows the variation of specific capacitance of undoped and Mn doped $CuO/Cu(OH)_2$ thin films as a function of cycle number. The repetitive charge/discharge cycling test of hybrid electrodes were carried out at 5 $mAcm^{-2}$ for 1000 cycles. All the Mn:doped $CuO/Cu(OH)_2$ electrode exhibits good cycling stability in the range from 88% - 92 % after 1000 cycles. The reason for good cycling stability would be unique 3D nanostructures of $Mn:CuO/Cu(OH)_2$ films which sustain the volume expansion of material during charging/discharging cycles [35].

Fig. 8 shows the Nyquist plots for undoped and Mn doped $Cuo/Cu(OH)_2$ electrodes in 1M $Na_2SO_4$ electrolyte within a frequency range of 1 Hz-10MHz at amplitude of 5 mV. EIS spectra are divided into three distinct regions based on the order of decreasing frequencies. The slope of the EIS curve in the low frequency range reflects the Warburg resistance, which describes the diffusion rate of redox material in the electrolyte. The higher value of slope in the case of 3% $Mn:CuO/Cu(OH)_2$ electrode over other $CuO/Cu(OH)_2$ electrode indicates higher electrolytic ion diffusion within the nanoflowers structure [36]. The phase angle of the impedance plots of undoped and Mn doped $CuO/Cu(OH)_2$ electrodes established to be higher than 45˚ in the low frequency range indicate diffusion controlled electrochemical capacitive behavior. The shorter line at lower frequency correlates to the shorter variations in ion diffusion path and easier movement of the ions within the pores. The diameter of semicircle in the high frequency range

represents the charge transfer resistance (Rct) of the electrode material resulting from the diffusion of ions. Here, the value of $R_{ct}$ for 3% Mn:CuO/$Cu(OH)_2$ is 5.31 Ω which is smaller than that for undoped (14.11 Ω) as well as 1% (13.41 Ω) and 5 % (14.75 Ω) Mn:CuO/$Cu(OH)_2$ electrodes, respectively indicating that nanoflowers-like structure is ideal for fast ion and electron transport, because the larger diameter semicircle reflects higher charge-transfer resistance value. The intercept on the real axis in the high frequency range provides the equivalent series resistance (ESR), which comprises the bulk resistance of the electrolyte, the inherent resistances of the electro-active material and the contact resistance at electrolyte/electrodeinterface [37, 38]. The values of ESR forCuO/$Cu(OH)_2$, 1% Mn:CuO/ $Cu(OH)_2$, 3% Mn:CuO/$Cu(OH)_2$ and 5% Mn:CuO/$Cu(OH)_2$ electrodes are found to be 3.7 Ω, 3.8 Ω, 3.2 Ω and 3.9Ω, respectively. Thus, here again, the hierarchical 3% Mn doped CuO/$Cu(OH)_2$ nanostructures assembled from thin nanoflowers demonstrate superior electrochemical properties, making them promising electrode materials for practical applications.

## 4. Conclusions

In conclusion, we have systematically investigated the effect of Mn incorporation on the supercapacitive properties of CuO/$Cu(OH)_2$ hybrid electrodes synthesized by SILAR method. Our results revealed the formation of hybrid CuO/$Cu(OH)_2$ thin films with significant morphological variation through Mn doping. Moreover, it is seen that Mn doping significantly alters the supercapacitive properties of hybrid CuO/$Cu(OH)_2$ electrodes. Later, the results suggest that at 3% Mn doping in CuO/$Cu(OH)_2$ electrodes with nanoflower-like nanostructure exhibits highest specific capacitance of 600 $Fg^{-1}$ at scan rate of 5 $mVs^{-1}$. In addition to this, these Mn:CuO/$Cu(OH)_2$ electrode shows excellent cycling stability in the range of 88 % - 92 % with

high specific energy (10-50 Wh/kg) and high specific power (0.7-3.1 kW/kg). Thus, present research efforts offer the novel system and improved hybrid Mn:CuO/$Cu(OH)_2$ composites for the synthesis of hybrid materials by simple SILAR method for the manufacture of supercapacitors.

**References**

[1] J. Wu, D. Xue, Cryst. Eng. Comm., 13 (2011) 1966

[2] (a) J. Zhao, Y. Zhang, T. Wang, P. Li, C. Wei, H. Pang, Adv. Mater. Interfaces, 2 (2015) 1400377 (b) Y. Zhang, C. Sun, P. Lu, K. Li, S. Song, D. Xue, Cryst. Eng. Comm., 14 (2012) 5892

[3] (a) D. P. Dubal, J. G. Kim, Y. Kim, R. Holze, C. D. Lokhande, W. B. Kim, Energy Technol. 2 (2014) 325 (b) J. C. Park, J. Kim, H. Kwon, H. Song, Adv. Mater., 21 (2009) 803

[4] J. Liu, H. Xia, D. Xue, L. Lu, J. Am. Chem. Soc., 131 (2009) 12086

[5] (a) D. P. Dubal, O. Ayyad, V. Ruiz, P. Gomez-Romero, Chem. Soc. Rev., 2015, DOI: 10.1039/C4CS00266K (b) J. Liu, D. Xue, Adv. Mater., 20 (2008) 2622

[6] G. R. Patzke, Y. Zhou, R. Kontic, F. Conrad, Angew. Chem., Int. Ed., 50 (2011) 826

[7] D. Barreca, G. Carraro, A. Gasparotto, C. Maccato, M. C. Yusta, J. L. G. Camer, J. Morales, C. Sada, L. Sanchez, ACS Appl. Mater. Interfaces, 4 (2012) 3610

[8] J. Liu, H. Xia, L. Lu, D. Xue, J. Mater. Chem., 20 (2010) 1506

[9] K. Chen, D. Xue, CrystEngComm, 2012, **14**, 8068-8075

[10] J. Xu, D. Xue, Acta. Mater., 55 (2007) 2397

[11] K. Chen, D. Xue, Nanosci. Nanotechnol. Lett., 4 (2012) 1

[12] (a) D. P. Dubal, P. Gomez-Romero, B. R. Sankapal, R. Holze, Nano Energy, 11 (2015) 377 (b) K. Chen, S. Song, D. Xue, Cryst. Eng. Comm., 15 (2013) 144

[13] W. Kang, F. Liu, Y. Su, D. Wang, Q. Shen, Cryst. Eng. Comm., 13 (2011) 4174

[14] S. Ko, J. Lee, H. S. Yang, S. Park, U. Jeong, Adv. Mater., 24 (2012) 4451

[15] V. D. Patake, S. S. Joshi, C. D. Lokhande, O. S. Joo, Mater. Chem. Phys.114 (2009) 6

[16] G. S. Gund, D. P. Dubal, D. S. Dhawale, S. S. Shinde, C. D. Lokhande, RSC Adv. 3 (2013) 24099

[17] D. W. Kim, K. Y. Rhee, S. J. Park, J. Alloys Compd. 530 (2012) 6

[18] G. Wang, J. Huang, S. Chen, Y. Gao, D. Cao, J. Power Sources 196 (2011) 5756

[19] D. P. Dubal, D. S. Dhawale, R. R. Salunkhe, V. S. Jamdade, C. D. Lokhande, J. Alloys.

Compd. 492 (2010) 26

[20] S. K. Shinde, D. P. Dubal, G. S. Ghodake, V. J. Fulari, RSC adv., 5 (2015) 4443

[21] S. K. Shinde, D. P. Dubal, G. S. Ghodake, D. Y. Kim, V. J. Fulari, J. Electroanal. Chem. 732 (2014) 80

[22] P. Chand, A. Gaura, A. Kumar, U. K. Gau, Appl. Surf. Sci., 307 (2014) 280

[23] W. Gao, S. Yang, S. Yang, L. Lv, Y. Du, Phys. Lett. A 375 (2010) 180

[24] J. S. Shaikh, R. C. Pawar, R. S. Devan, Y. R. Ma, P. P. Salvi, S. S. Kolekar, P. S. Patil, Electrochim. Acta 56 (2011) 2127

[25] M. Ivilla, M. E. Overberg, C. R. Abernathy, D. P. Norton, A. F. Hebard, N. Theodoropoulou, J. D. Budai, Solid State Electronics., 47 (2003) 2215

[26] T. V. Thi, A. K. Rai, J. Gim, J. Kim, Appl. Surf. Sci., 305 (2014) 617

[27] L. J. Chen, G. S. Li, L. P. Li, J. Therm. Analys. Calorimetry, 91 (2008) 581

[28] K. Borgohain, J. B. Singh, M. V. R. Rao, T. Shripathi, S. Mahamuni, Phys. Rev. B, 61 (2000) 11093

[29] S. K. Shinde, J. V. Thombare, D. P. Dubal, V. J. Fulari, Appl. Surf. Sci., 282 (2013) 561

[30] S. K. Shinde, G. S. Ghodake, D. P. Dubal, G. M. Lohar, D. S. Lee, V. J. Fulari, Ceram Int., 40 (2014) 11519

[31] S. K. Shinde, D. P. Dubal, G. S. Ghodake, V. J. Fulari, Mater. Lett. 126 (2014) 17

[32] D. P. Dubal, G. S. Gund, R. Holze, C. D. Lokhande, J. Electroanal. Chem., 712 (2014) 4039

[33] Y. K. Hsu, Y. C. Chen, Y. G. Lin, J. Electroanal. Chem., 673 (2012) 43

[34] G. S. Gund, D. P. Dubal, S. S. Shinde, C. D. Lokhande, ACS Appl. Mater. Interfaces, 6 (2014) 3176

[35] J. Zhao, J. He, M. Sun, M. Qua, H. Pang, Chem. Front., 2 (2015) 129

[36] (a) Y. Gao, J. Zhao, Z. Run, G. Zhang, H. Pang, Dalton Trans., 43 (2014) 170, (b) L. Mai, H. Li, Y. Zhao, L. Xu, X. Xu, Y. Luo, Z. Zhang, W. Ke, C. Niu, Q. Zhang, Sci. Rep., 3 (2013) 1718

[37] J. M. Luo, B. Gao, X. G. Zhang, Mater. Res. Bull., 43 (2008) 1119

[38] A. K. Singh, D. Sarkar, G. G. Khan, K. Mandal, ACS Appl. Mater. Interfaces, 6 (2014) 4684

**Fig caption**

**Fig. 1** XRD patterns of the undoped and Mn doped $CuO/Cu(OH)_2$ thin films on stainless steel (SS) substrates

**Fig. 2** FTIR spectra of undoped and Mn doped $CuO/Cu(OH)_2$ samples

**Fig. 3** Scanning electron micrographs of (a, b) undoped $CuO/Cu(OH)_2$ and (c, d) 1 % Mn, (e, f) 3 % Mn, (g, h) 5 % Mn doped $CuO/Cu(OH)_2$ thin films, at two different magnifications, respectively. Insert of figure shows the corresponding Energy dispersive X-ray (EDAX) spectra of undoped and Mn doped $CuO/Cu(OH)_2$ thin films.

**Fig. 4** Plausible mechanism for the development of different nanostructures of undoped and Mn doped $CuO/Cu(OH)_2$ with special nanostructures such as nanopetals, nanoflakes and nanoflowers.

**Fig. 5** (a-c) Cyclic voltammetry (CV) curves of different percentage of Mn doped $CuO/Cu(OH)_2$ electrodes at different scanning rates, and (d) Variation of specific capacitance of $Mn:CuO/Cu(OH)_2$ with scan rate.

**Fig. 6** (a-c) Galvanostatic charge/discharge curves of Mn doped $CuO/Cu(OH)_2$ hybrid electrodes at different current densities, (d) Ragone plot suggesting the good values of specific energy and specific power for undoped and $Mn:CuO/Cu(OH)_2$ electrodes.

**Fig. 7** Variation of specific capacitance of undoped and Mn doped CuO/$Cu(OH)_2$ hybrid electrode as a function of cycles

**Fig. 8** Nyquist impedance plots for the undoped and Mn doped CuO/$Cu(OH)_2$ hybrid electrodes in frequency range of 1 Hz to10 MHz with AC amplitude of 5 mV.

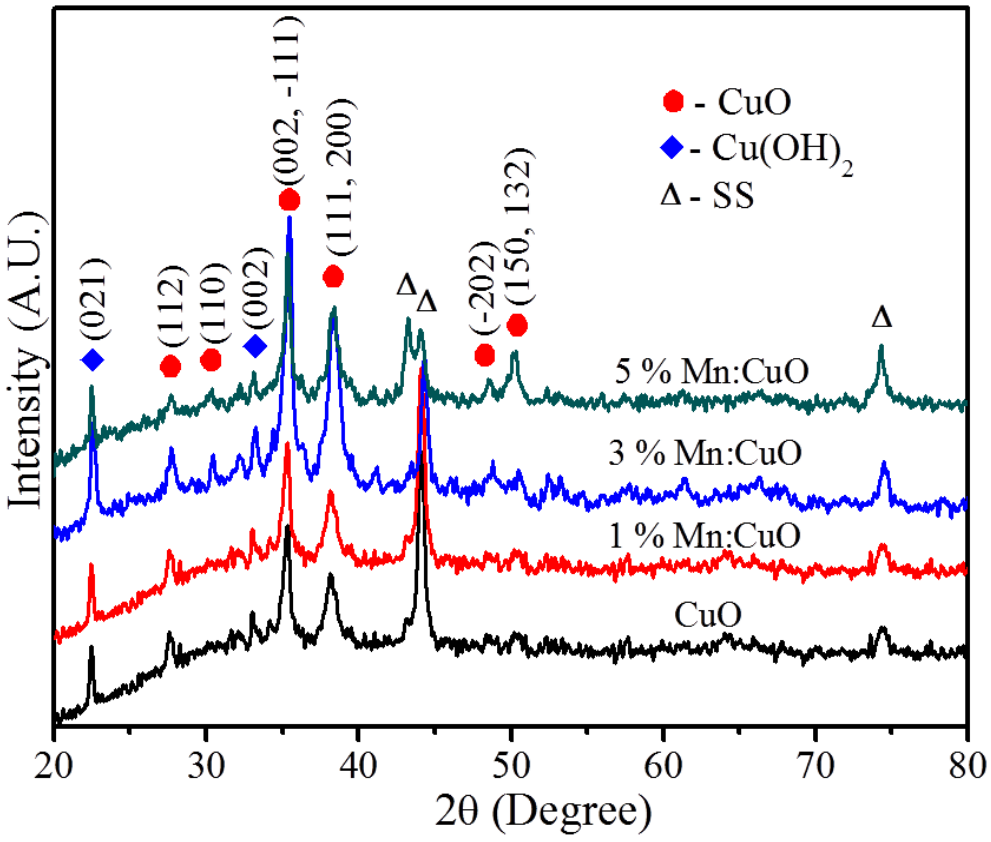
Intensity (A.U.)
2θ (Degree)
20
30
40
50
60
70
80
(021)
(112)
(110)
(002)
(002, -111)
(111, 200)
Δ
Δ
(-202)
(150, 132)
Δ
● - CuO
◆ - Cu(OH)2
Δ - SS
5 % Mn:CuO
3 % Mn:CuO
1 % Mn:CuO
CuO

**Fig. 1**

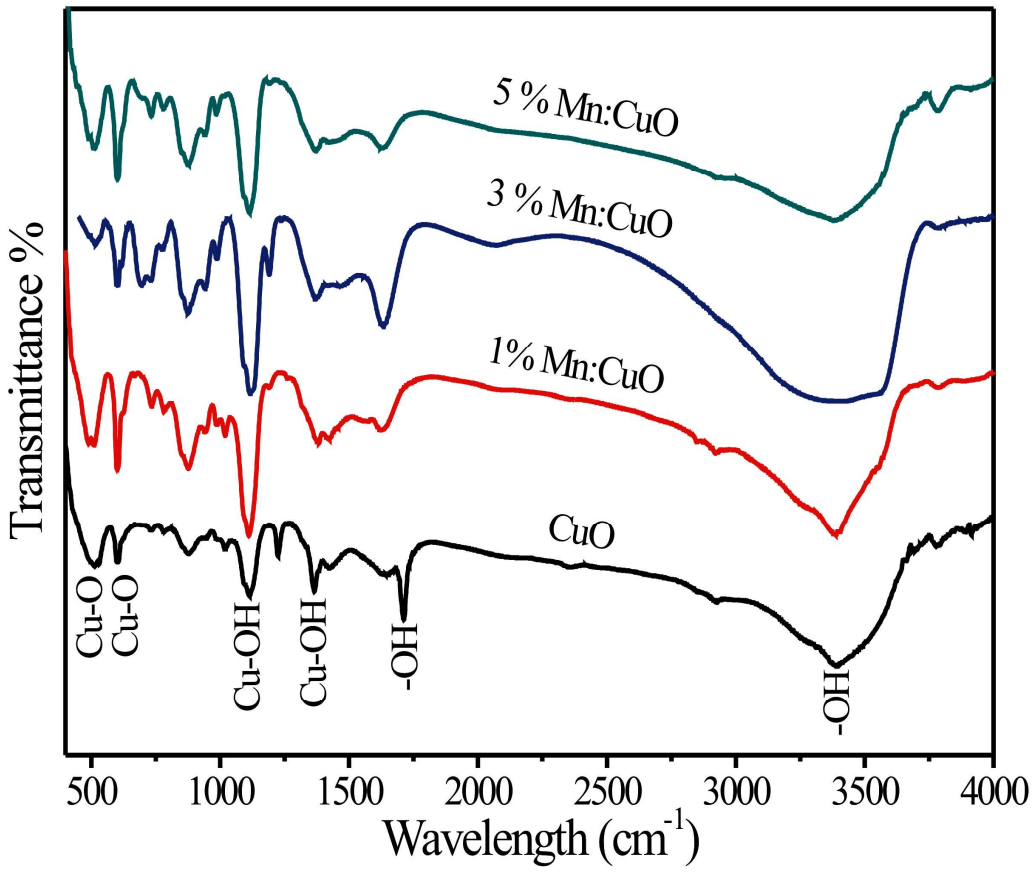
5 % Mn:CuO
3 % Mn:CuO
1% Mn:CuO
CuO
Cu-O
Cu-O
Cu-OH
Cu-OH
-OH
-OH
Transmittance %
500
1000
1500
2000
2500
3000
3500
4000
Wavelength (cm-1)

**Fig. 2**

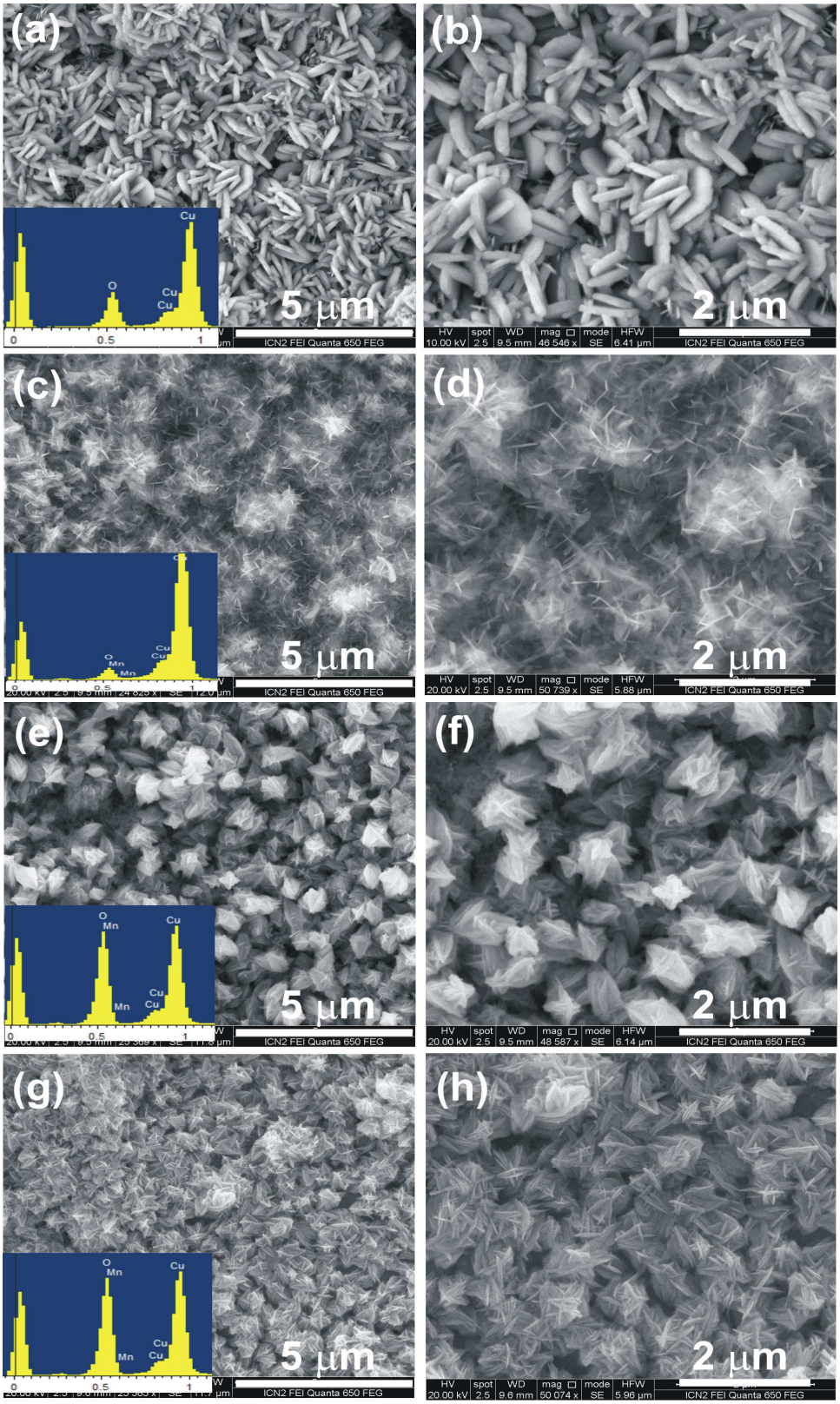
(a)
O
Cu
Cu
Cu
0
0.5
1
5 μm
ICN2 FEI Quanta 650 FEG
(b)
HV spot WD mag mode HFW
10.00 kV 2.5 9.5 mm 46 546 x SE 6.41 μm
2 μm
ICN2 FEI Quanta 650 FEG
(c)
5 μm
ICN2 FEI Quanta 650 FEG
(d)
HV spot WD mag mode HFW
20.00 kV 2.5 9.5 mm 50 739 x SE 5.88 μm
2 μm
ICN2 FEI Quanta 650 FEG
(e)
O
Mn
Cu
Mn
Cu
Cu
0
0.5
1
5 μm
ICN2 FEI Quanta 650 FEG
(f)
HV spot WD mag mode HFW
20.00 kV 2.5 9.5 mm 48 587 x SE 6.14 μm
2 μm
ICN2 FEI Quanta 650 FEG
(g)
O
Mn
Cu
Mn
Cu
Cu
0
0.5
1
5 μm
ICN2 FEI Quanta 650 FEG
(h)
HV spot WD mag mode HFW
20.00 kV 2.5 9.6 mm 50 074 x SE 5.96 μm
2 μm
ICN2 FEI Quanta 650 FEG

**Fig. 3**

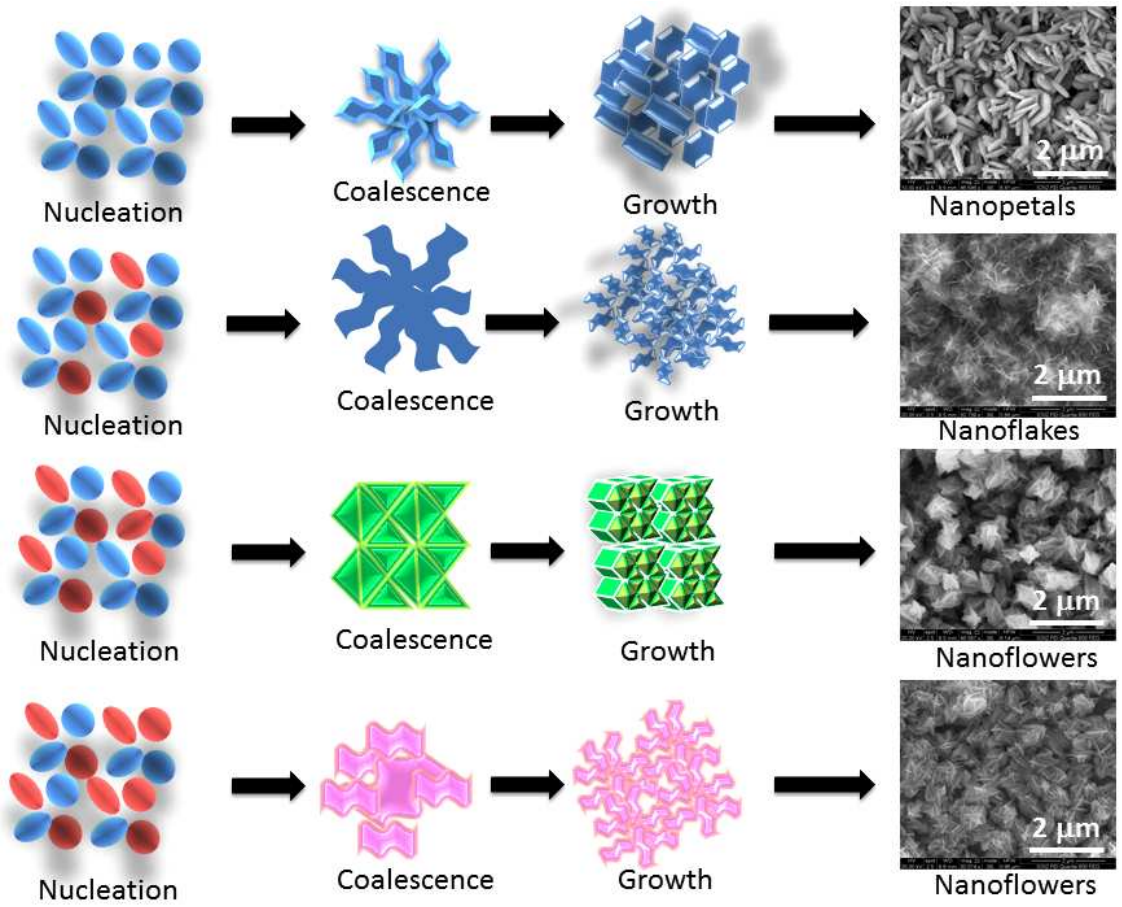
Nucleation
Coalescence
Growth
2 μm
Nanopetals
Nucleation
Coalescence
Growth
2 μm
Nanoflakes
Nucleation
Coalescence
Growth
2 μm
Nanoflowers
Nucleation
Coalescence
Growth
2 μm
Nanoflowers

**Fig. 4**

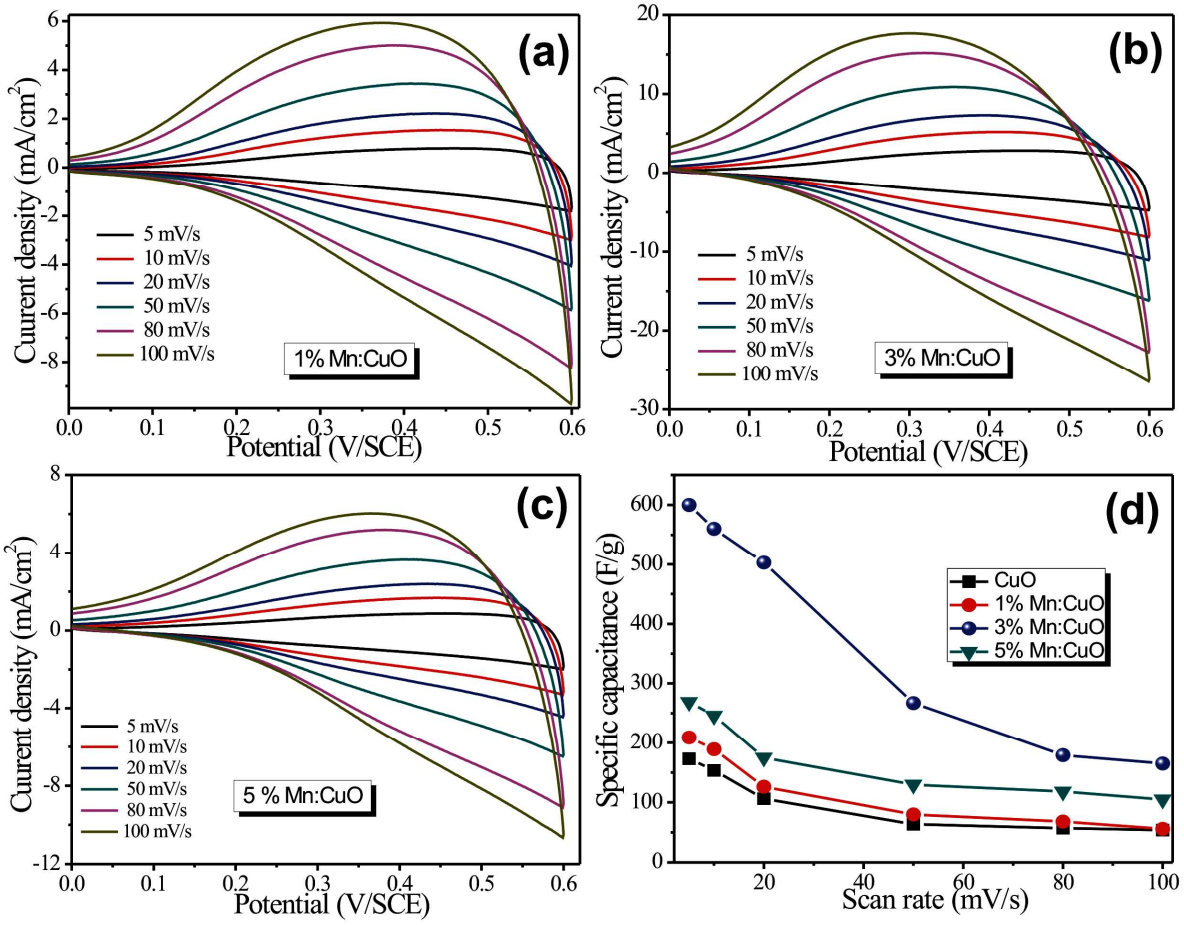
(a)
Cuurent density (mA/cm$^2$)
Potential (V/SCE)
5 mV/s
10 mV/s
20 mV/s
50 mV/s
80 mV/s
100 mV/s
1% Mn:CuO
(b)
Current density (mA/cm$^2$)
Potential (V/SCE)
3% Mn:CuO
(c)
Cuurent density (mA/cm$^2$)
Potential (V/SCE)
5 % Mn:CuO
(d)
Specific capacitance (F/g)
Scan rate (mV/s)
CuO
1% Mn:CuO
3% Mn:CuO
5% Mn:CuO

**Fig. 5**

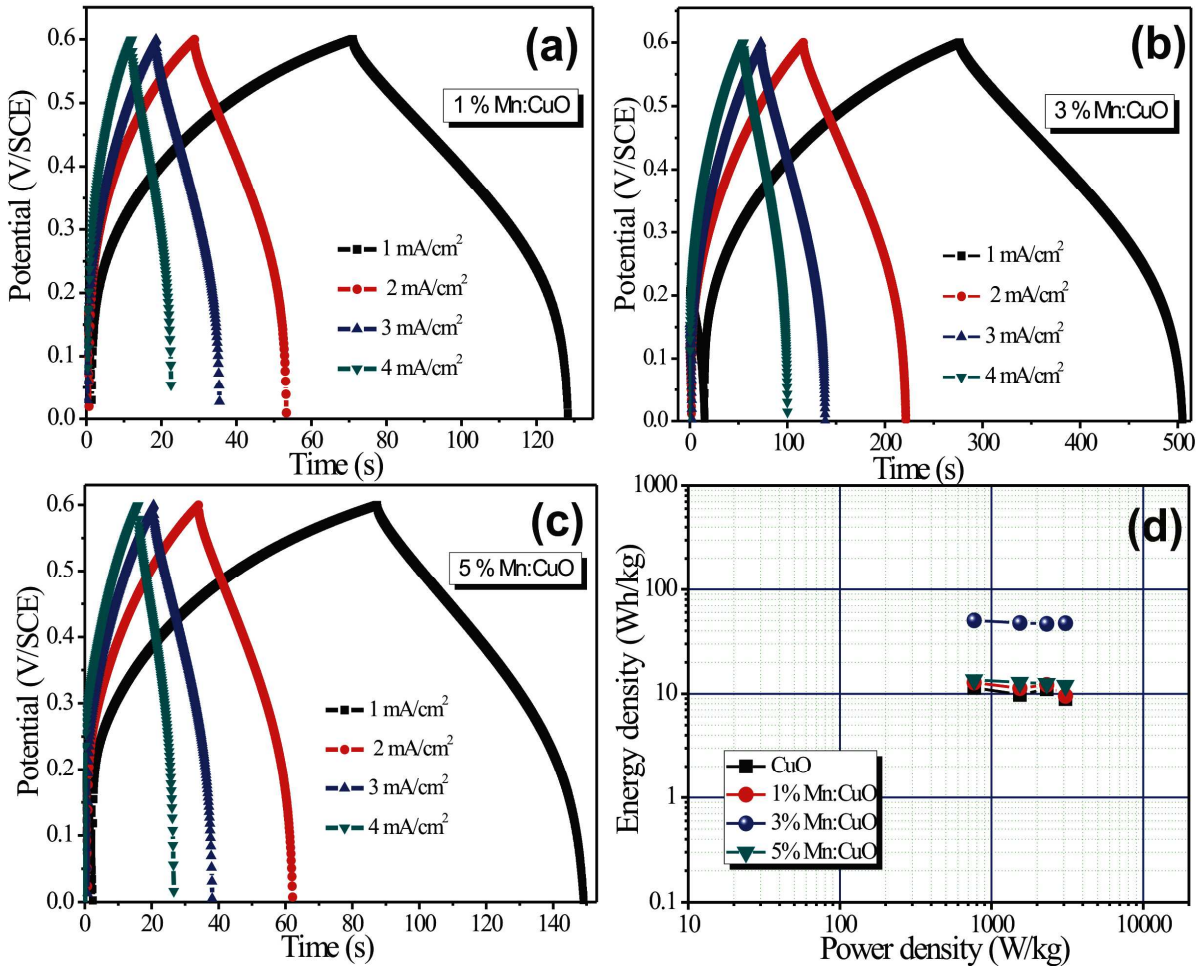
(a)
1 % Mn:CuO
Potential (V/SCE)
Time (s)
1 mA/cm2
2 mA/cm2
3 mA/cm2
4 mA/cm2
(b)
3 % Mn:CuO
(c)
5 % Mn:CuO
(d)
Energy density (Wh/kg)
Power density (W/kg)
CuO
1% Mn:CuO
3% Mn:CuO
5% Mn:CuO

**Fig. 6**

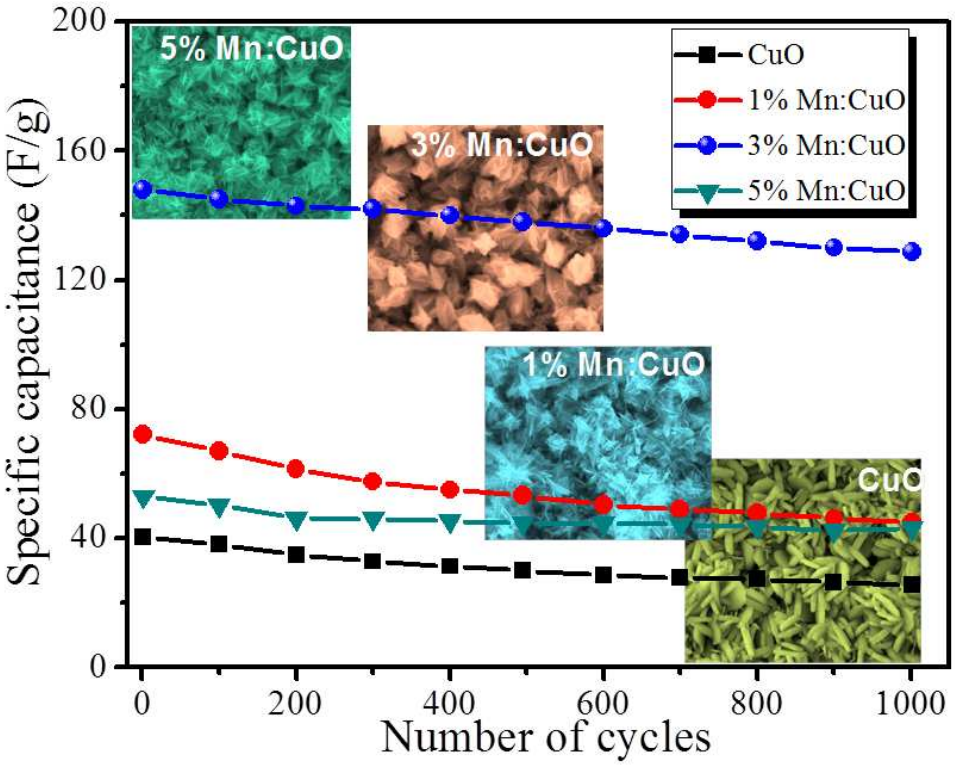
5% Mn:CuO
3% Mn:CuO
1% Mn:CuO
CuO
CuO
1% Mn:CuO
3% Mn:CuO
5% Mn:CuO
Specific capacitance (F/g)
Number of cycles
0
40
80
120
160
200
0
200
400
600
800
1000

**Fig. 7**

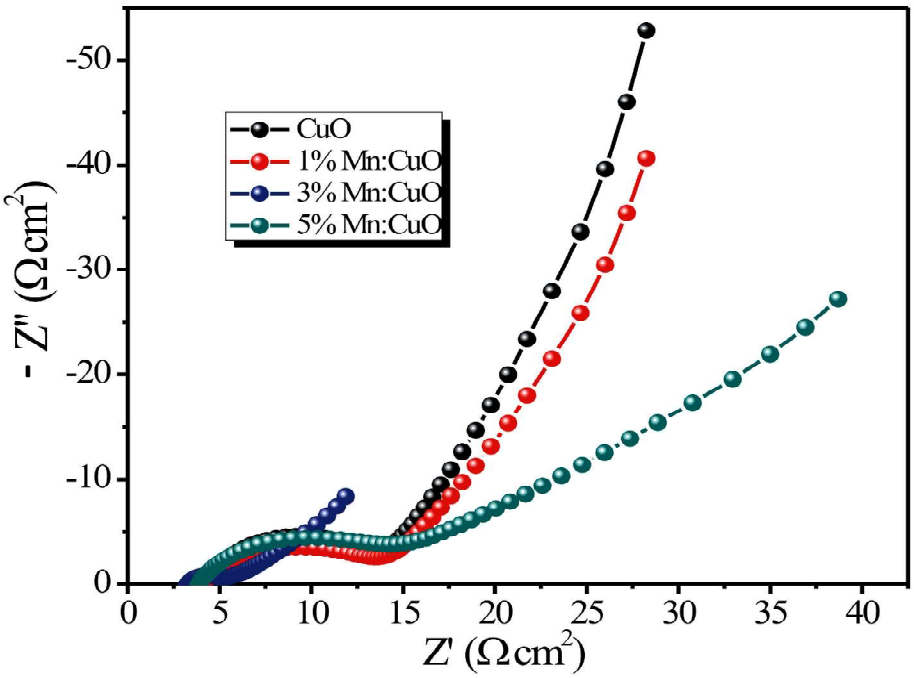
CuO
1% Mn:CuO
3% Mn:CuO
5% Mn:CuO
- Z'' (Ωcm²)
Z' (Ωcm²)
0
-10
-20
-30
-40
-50
0
5
10
15
20
25
30
35
40

**Fig. 8**

**Graphical abstract:**

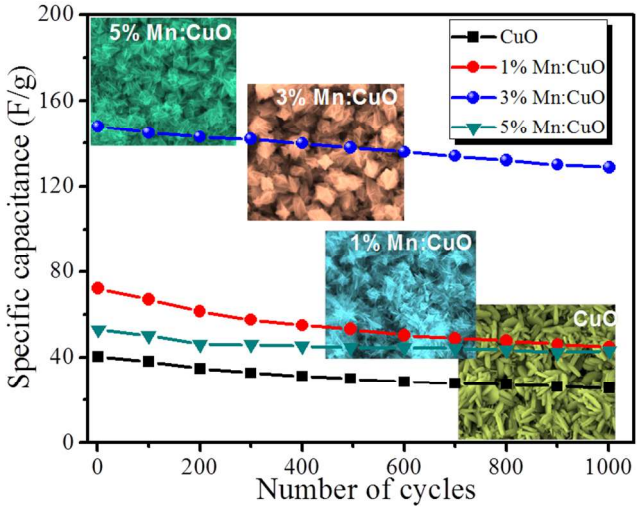


Variation of specific capacitance of undoped and Mn doped CuO/$Cu(OH)_2$ hybrid electrodes with corresponding SEM